University of Baghdad
College of Engineering
JE
JOURNAL OF ENGINEERING

Journal of Engineering

journal homepage: www.jcoeng.edu.iq

Volume 32 Number 3 March 2026

Surface Changes of Al-Hammar Marsh using Remote Sensing and Geographic Information Systems

Dina Ali Jasim *, Alaa D. Salman

Department of Surveying, College of Engineering, University of Baghdad, Baghdad, Iraq

ABSTRACT

The study examines temporal variation in water levels by calculating the surface area of the Al-Hammar Marsh in southern Iraq over 11 years (2013–2023), because of the consistent Landsat-8 and Landsat-9 data. Because it represents years of remarkable hydrological diversity in Iraq, it provides a trusted assessment for the surface changes of Al-Hammar marsh by using geographic information systems and remote sensing. The change in the surface was determined by utilizing supervised classification (maximum likelihood) to classify the region. Water and vegetation were the two land cover classes that we determined using ArcMap software. Then the thematic maps were created by the same software. The resulting signalize that the surface area changed a lot over the study years, where the large area was recorded in 2019 (1144 km^2), and the small area was recorded in 2023 (295 km^2). The accuracy assessment showed the supervised classification provided high trust, with overall accuracy ranging between 87 % to 98% and a kappa coefficient ranging between 0.88 and 0.98, which indicated strong agreement.

Keywords: Satellite images, Supervised classification method, Surface area.

1. INTRODUCTION

The big portion of Iraq's water bodies are marshes. The Mesopotamian Basin is home to the Iraqi marshlands, which cover about 30,000 km^2 **(Davidson et al., 2020).** Remote sensing is a widely used technology for obtaining information about land cover and surface characteristics without direct contact with the target **(Schowengerdt, 2006)**. Satellite image provides a constant tool to monitor the environmental changes that the hydrological and climatic condition influenced in it, as in several studies (**Xiao et al., 2004; Campbell and Wynne, 2011)**. Wetlands represent 3–6 % of the Earth's surface and provide an vary environment functions **(Ghobadi et al., 2012; Malekmohammadi and Blouchi, 2014)**. The Iraqi marshes are the most important wetlands in the world, depending on the changes in season and inflows from the Tigris and Euphrates **(Yacoub, 1981)**. They extend between the provinces of Basrah and Dhi Qar **(Al-Rubaie, 2008; Muhsin, 2017)**. Over the past four

*Corresponding author
Peer review under the responsibility of University of Baghdad.
https://doi.org/10.31026/j.eng.2026.03.04

Article received: 26/07/2025
Article revised: 02/02/2026
Article accepted: 16/02/2026
Article published: 01/03/2026

decades, marshes have experienced substantial shrinkage due to upstream dams, reduced inflows, and climatic pressures **(Shimal and Shaban, 2019)**. Remote sensing and GIS are strong tools for estimating long-term ecological changes. Landsat 8/9 imagery allows consistent monitoring, especially for classification, accuracy assessment, change detection, and map production **(Liu and Mason, 2016)**. Integration of geospatial datasets and decision-making is supported by GIS (**Nizeyimana, 2005; Childs, 2004; Babu, 2016)**. Previous remote sensing studies have provided useful insight into the land cover dynamics of Al-Hammar marsh. For example **(Dhaidan et al., 2021)** used spectral indices (NDVI, NDMI, NDWI) to analyze land cover variation between 2013 and 2020, and (**Al-Maliki et al., 2022)** classified the region into six categories during the years 2017 and 2019. Many studies used Landsat and Sentinel to classify the region into three classes: water, vegetation, and dry land **(Muhsin, 2017; Al-Atbee et al., 2019; Wahaab et al., 2022)**. Despite numerous contributions, a long-term, consistent, decade-scale assessment of the Al-Hammar Marsh using harmonized Landsat 8/9 datasets and supervised classification remains limited. Previous studies did not provide a continuous 11-year evaluation capable of capturing hydrological variability, trends in surface area, and the cumulative effects of climate and water-management conditions.

The present study aims to fill this gap; the main objectives are:

1. To identify and classify the land-cover types in the Al-Hammar Marsh using supervised maximum likelihood classification.
2. To analyze temporal changes in water and vegetation cover during the period 2013–2023 using Landsat 8/9 imagery.
3. To quantify variations in the surface area of the marsh and evaluate long-term hydrological trends.

2. MATERIAL AND METHODOLOGY

2.1 Study Area

Al-Hammar Marsh is the largest wetland in southern Iraq, extending from Al-Nasiriyah in the west to the Shatt Al-Arab River in the east showed in **Fig. 1**. It is divided into western Hammar and eastern, which distic hydrological system **(Al-Atbee et al., 2019)**. The western section, situated in Thi-Qar Province, covers approximately 1326 km^2 and receives water primarily from the Euphrates River and the Main Outfall Drain (MOD), and some branches such as Al-Kurmashia, Um Nakhal, and Al-Hamedy. In contrast, the eastern section within Basra Governorate is influenced by tidal inflows from the Shatt Al-Arab **(Wahaab et al., 2022).** Historically, the marsh covers an area of approximately 2800 km^2 in normal conditions and may reach 4500 km^2 in flood season, with depths between (1.8 and 3) m **(Aqrawi and Evans, 1994; Yacoub, 1981).** Al-Hammar marsh forms one of the three main wetlands in Iraq, in addition, there is central and Hawizeh marshes **(Hussein et al., 2018; Al-Rubaie, 2008).** Over recent decades, hydrological alterations, dam construction, and reduced river inflow have significantly modified the extent and ecological characteristics of the marsh **(Shimal and Shaban, 2019)**.

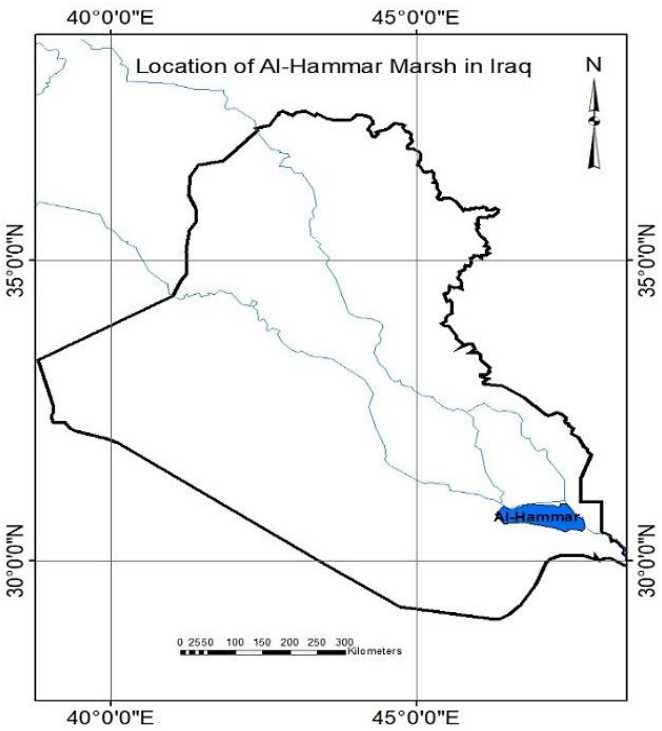

Figure 1. Study area (Al-Hammar marsh)

2.2 Data Use

Landsat sensors offer a spatial resolution of 30 m for visible, near-infrared, and shortwave infrared bands, which is suitable for regional-scale wetland monitoring and surface-water mapping **(Irons et al., 2012; Roy et al., 2022)**. 44 images from Landsat 8/9 were used in this study(4 scenes × 11 years = 44 images), which are required to cover the study area for eleven years from 2013 to 2023. **(Pritt et al., 2017)** shown that because of its radiometric quality and spatial resolution, Landsat 8/9 OLI data offer trustworthy spectral information for supervised land cover categorization. The study verified that when suitable preprocessing and training samples are used, conventional statistical classifiers such as the Maximum Likelihood Classifier remain useful for mapping land cover classes. All images were obtained from the Landsat Collection 2 Level 2 products, which provide atmospherically and radiometrically correct surface reflectance.

The dataset includes OLI reflective bands and TIRS thermal bands, which were processed and analyzed for classification and change-detection purposes. These images were obtained free of charge from the USGS website. The Hammar Marsh Landsat data from 2013 to 2023 are inconsistent, so multiple images are needed to cover the area. Landsat data is often used to classify land cover since it has a spatial resolution of 30 m, a revisit interval of 16 days, and a spatial coverage of 185×185 km^2.

2.3 Methodology

All image processing, classification, and area calculations were performed using ArcMap 10.8 following standard GIS and remote-sensing procedures **(Meng et al., 2022).** Then, the images were merged (four scenes for each study year) using the mosaic technique to obtain complete coverage of the study area. After that, the study area was clipped using the Extract by Mask tool in ArcMap. These operations are in the pre-processing stage, while the processing stage includes classifying the image using supervised classification (maximum

likelihood classification) and the production of thematic maps of the region, after classifying it into two categories: water and green areas. In the post-processing stage, the surface area of the Al-Hammar Marsh was measured over eleven years, showing how it changed from 2013 to 2023. **Fig. 2** depicts how the research was done.

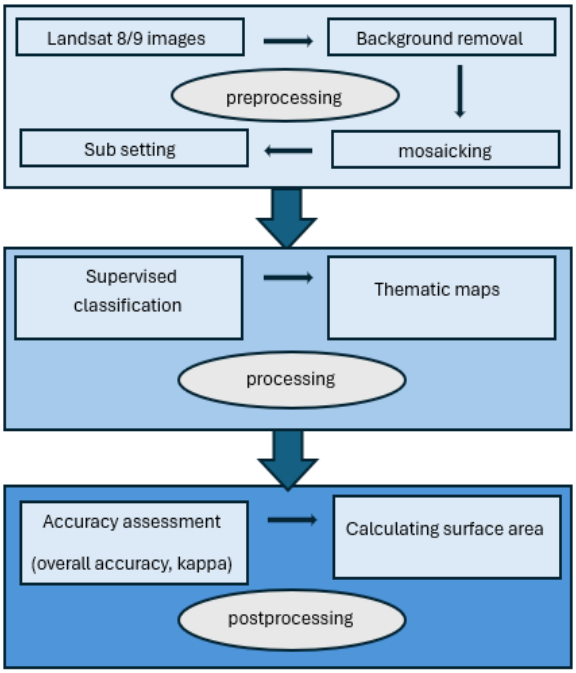

Figure 2. The research methodology**.**

2.4 Data Integration of GIS

Remote sensing is the principal source of several types of thematic data that are important for GIS analysis, such as data on land use and land cover. Aerial and Landsat images are also often used to check how land cover is spread out and to add new geographical features to existing ones. The advent of remote sensing technologies and image processing software has greatly enhanced the significance of remote sensing in Geospatial Information Technologies (GIS) **(Jenness and Wynne, 2006)**. A geographic information system can link or combine information that is hard to connect in any other way. So, the system lets you use your own sets of variables to make and study new ones. For instance, GIS technology can be used to merge topographic records with hydrographic data to find out which streams can handle particular levels of river flow. You can use GIS to estimate how many nutrients will drain off the surface of each marsh. ArcGIS Desktop 10.8 also emphasizes integration with other Esri products and services, including ArcGIS Online and ArcGIS Enterprise. This allows for seamless data sharing, collaboration, and access to a wealth of online resources and datasets. Additionally, the version introduces enhancements in geoprocessing performance, improved user interface elements, and expanded support for data types, ensuring that users have the tools they need to make informed decisions based on spatial data. GIS software can create thematic maps that illustrate changes in soil bearing capacity. It also has many applications, including mapping and distributing certain soil properties for use in construction projects, as it is a function of geographic coordinates **(Sabaa et al., 2023).** Three primary methods for integrating remote sensing and GIS technologies to mutually enhance their capabilities are: (1) remote sensing is used to collect data that may be used in GIS; (2) GIS data is used to

improve the products that come from remote sensing; and (3) remote sensing and GIS are used together for modelling and analysis. This section discusses the three methods and how integration can be used in cities **(Nizeyimana, 2005)**.

2.5 Preprocessing of Landsat 8/9 Image

The image has been processed for geometric and radiometric errors in order to get rid of distortions within the image and to obtain data that matches the reality to prepare the images for further processing and analysis **(Lillesand et al., 2015).** Set 2 is the result of the USGS's reprocessing of the stored Landsat 8/9 data. To make these images usable immediately after processing, this set increased geometric radiometric calibration, introduced ground control and elevation data sets, added Level 2 surface reflectance and surface temperature products, and enhanced atmospheric correction **(Meng et al., 2022)**. The preprocessing method also includes employing a mosaic approach to combine the images and a sub setting step to obtain the study area ready for processing.

2.5.1 Mosaic Technique

Satellite data provides a credible and accurate source of knowledge about the patterns of land cover dynamics from the 1970s, because there are no chronological land cover maps for such a vast area of the three major marshes in southeastern Iraq **(Storey and Choate, 2014)**. Multiple Landsat scenes were mosaicked to ensure full spatial coverage of the marsh area due to the large extent of the study region **(Saleh, 2012)**. The two **Figs. 3 and 4** below illustrate the mosaic process of images covering the study area.

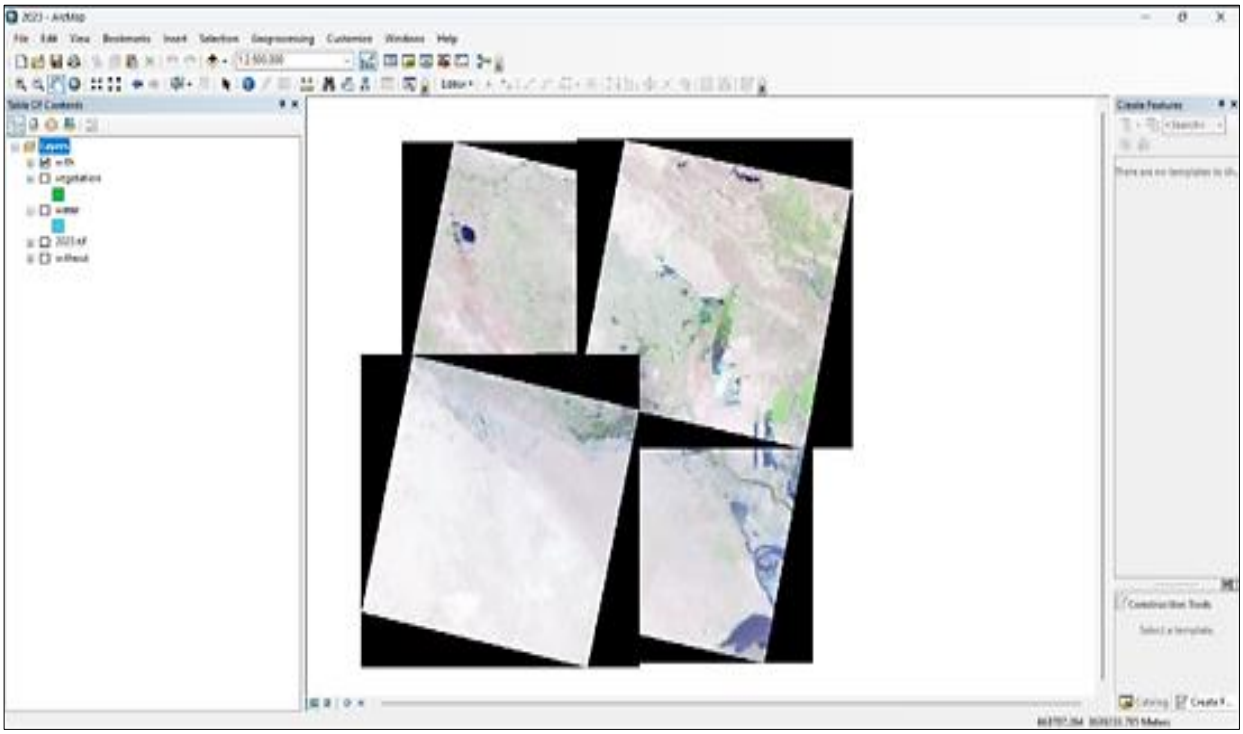

Figure 3. Satellite images after mosaicking and processing of AL-Hammar Marsh.

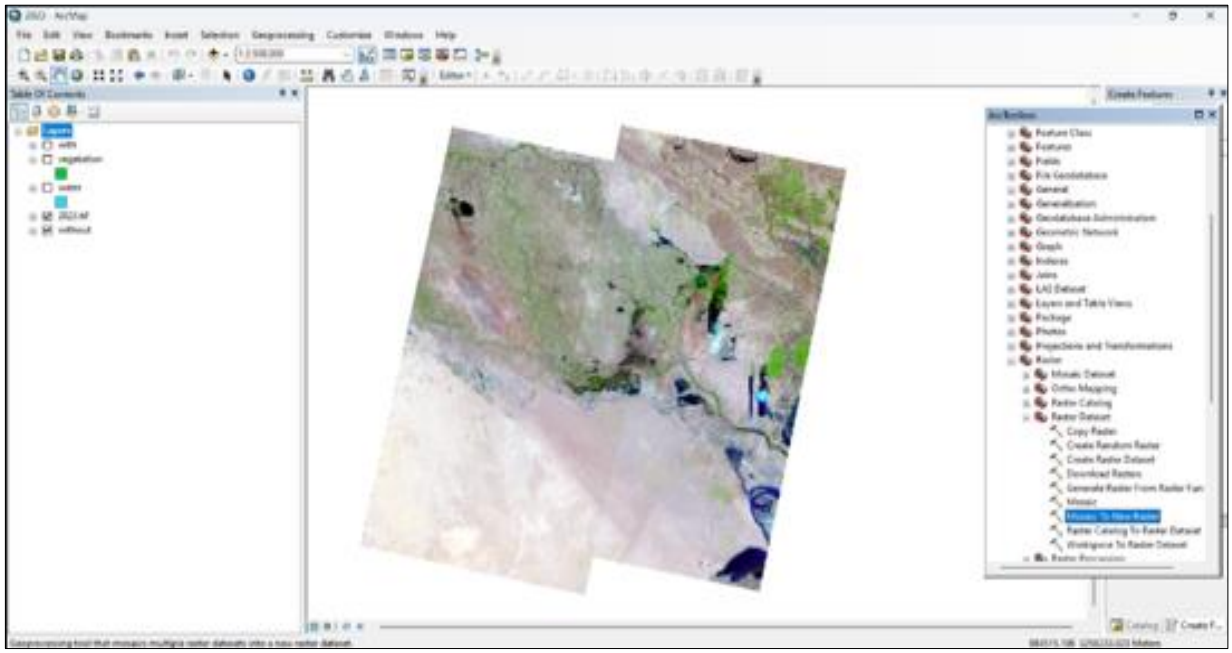

Figure 4. Satellite images after mosaicking and processing of AL-Hammar Marsh.

2.5.2 Image Sub-Setting of the Study Area

Sub-setting is defined as taking out part of a large file to form a single or several small files. As the selected study area is part of a large satellite image, it is necessary to perform this process to reduce the image file size for covering the study area only and to simplify and accelerate the analysis to obtain the results required as soon as possible **(Jonsson, 2015)**. The following **Fig. 5** shows the sub- setting process and how to select training samples in the supervised classification process using ArcMap (10.8).

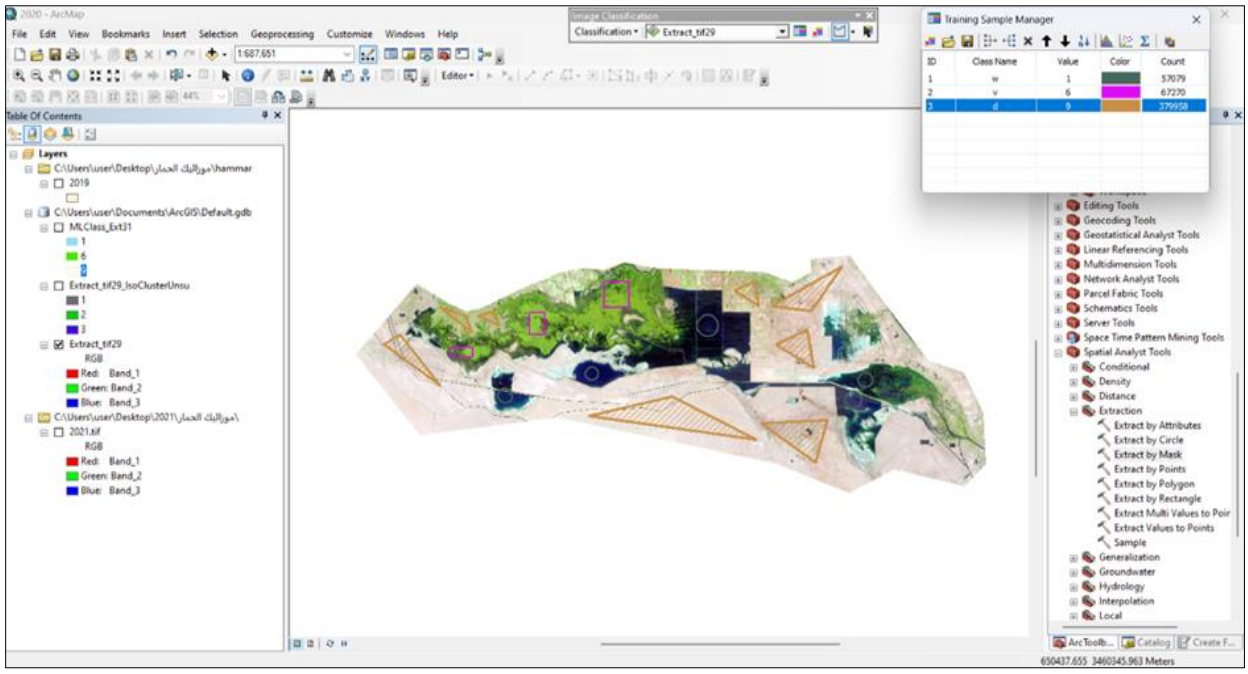

Figure 5. The technique of sub-setting in ArcMap (10.8).

2.6 Image Processing

Satellite images require specific processing steps before information retrieval in subsequent processing operations becomes possible. These operations include supervised classification.

2.6.1 Supervised Classification Using Maximum Likelihood

People normally consider classification to be the process of putting the pixels together with the important classes. This classification method is generally executed through a multi-step workflow **(Dhingra and Kumar, 2019)**. According to this source **(Jensen and Lulla, 1987)**, supervised classification is the process by which the user assigns spectral signatures to classified classes, such as water and green areas, and then the software assigns each pixel in the image to the class type that is most comparable. Supervised classification is the process most frequently used for quantitative analyses of remote sensing image data **(Richards and Jia, 2006)**. The most common way to do quantitative analysis of remote sensing picture data is to use supervised classification. It depends on employing the right algorithms to categories the pixels in an image as types or classes of ground covers. This phase is the training step. After training, the classifier uses the trained parameters to give each pixel in the image a label. The quality of a supervised classification is contingent upon the quality of the training sites. Maximum likelihood classification is the most prevalent type of supervised classification **(Sabaa et al., 2023)**. Many techniques can do this. Some use probability distribution models for the classes of interest, while others divide the multispectral space into class-specific regions using optimally situated surfaces **(Richards and Jia, 2006)**. The classification procedure entails putting each pixel in the satellite images into one of two groups, depending on its spectral features and the patterns that were chosen during the training phase. The most popular way to do the classification procedure in this paper is with maximum likelihood classification. The classification process includes assigning each pixel in the satellite images to one of the two categories based on its spectral properties and the patterns selected from the training phase. As shown in **Fig. 5**, which shows the sub-setting process, the training samples were selected according to the region.

2.6.2 Classification Accuracy Assessment

Accuracy assessment is an important step in remote sensing data processing, as it determines the values of the resulting data for the user and makes the data more reliable and high-quality. This is done by classifying each pixel in the image with its corresponding real-world data **(Jensen and Lulla, 1987; Congalton, 1991; Campbell and Wynne, 2011)**. To assess the reliability of the classification, the ambiguity matrix was used by comparing it with the ground truth data for both land use maps and land cover for the years 2013 to 2023, using terrestrial truth areas of interest. It will also be mentioned in the results, where the table will show the classification accuracy percentage for each thematic map for eleven years. ArcMap 10.8 was used to build the confusion matrix. By leveraging these metrics to assess accuracy **(Jenness and Wynne, 2006)**. The reliability of the marsh surface area classification was assessed, providing insights into the quality and validity of the resulting classified land cover map.

2.6.3 Surface Area Estimation and Change Detection

To identify changes in the surface area of Al Hammar Marsh, Landsat 8-9 images were used. The strategy was to process and analyze these images using the GIS program. By determining the number of pixels that belong to water-related classes in classified Landsat imagery,

surface water and wetland regions can be precisely estimated. The study verified that a dependable method for tracking changes in wetland surface area over time is post-classification pixel-based area calculation **(Hu et al., 2021).** The displayed images have a high degree of spatial accuracy, which makes detecting any change and drawing maps possible and accurate. After analysis, these images were subjected to a transformation process to produce maps that reflect the selected research area, i.e., converting them to vector data using the ArcMap 10.8 program. The program computed the area of Al Hammar Marsh for both water and green regions. The method of change detection after classification is the most straightforward way to look for changes based on categorization. After classifying photos, a comparison method can be used to compare two or more images. This method includes a classification step and a comparison phase**(Xu et al., 2008)**. The fundamental premise of employing remote sensing data for change detection is that alterations in land cover must lead to variations in radiance values, and these radiance changes, attributable to land cover modifications, must be significant in comparison to radiance fluctuations induced by other sources **(Singh, 1989)**.

4. RESULTS AND DISCUSSION

The marshes in Iraq are a crucial source of surface water. The findings of this study reveal significant temporal changes in the Al-Hammar Marsh between 2013 and 2023, influenced by hydrological variations, climatic conditions, and human activities. **Figs. 6–16** present thematic classification maps of the study area, showing two main land cover categories: water and vegetation.

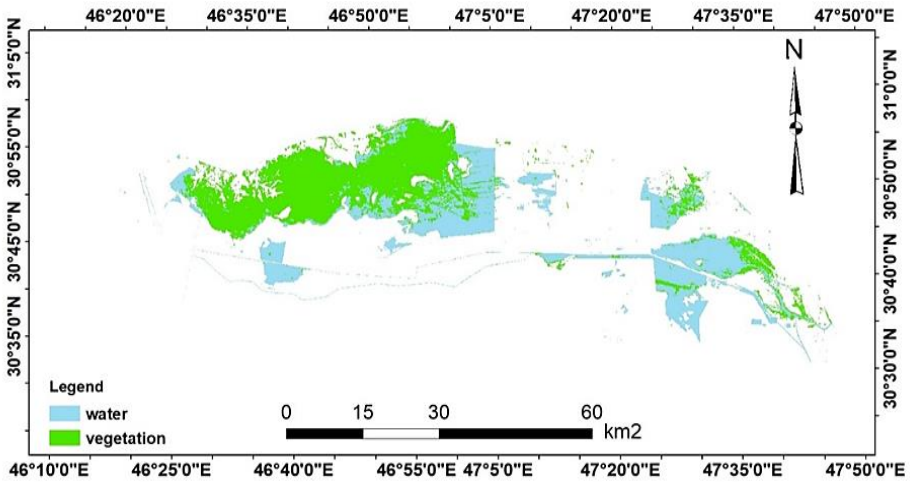

Figure 6. Thematic classification map of the study area for 2013 showing the spatial distribution of water (601.91 km^2) and vegetation (693.97 km^2) at a scale of 1:600,000.

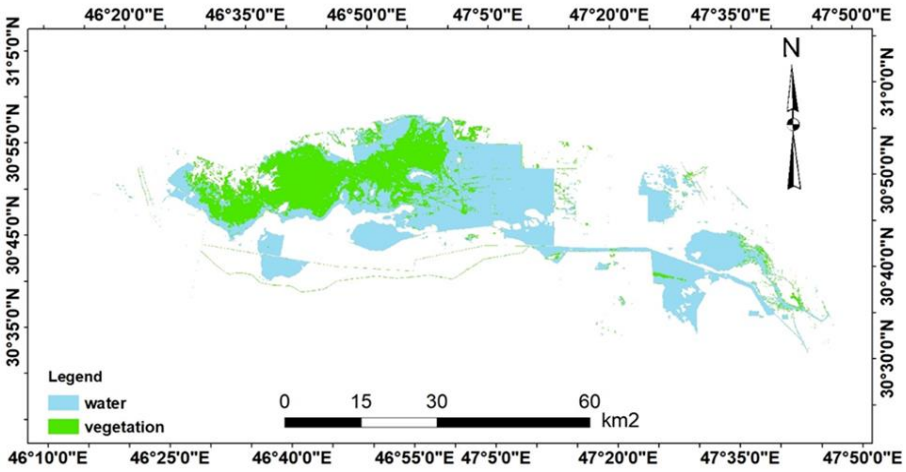

Figure 7. Thematic classification map of the study area for 2014, displaying water 1004.28 km^2 and vegetation 523.98 km^2, illustrating the increase in water area compared to 2013.

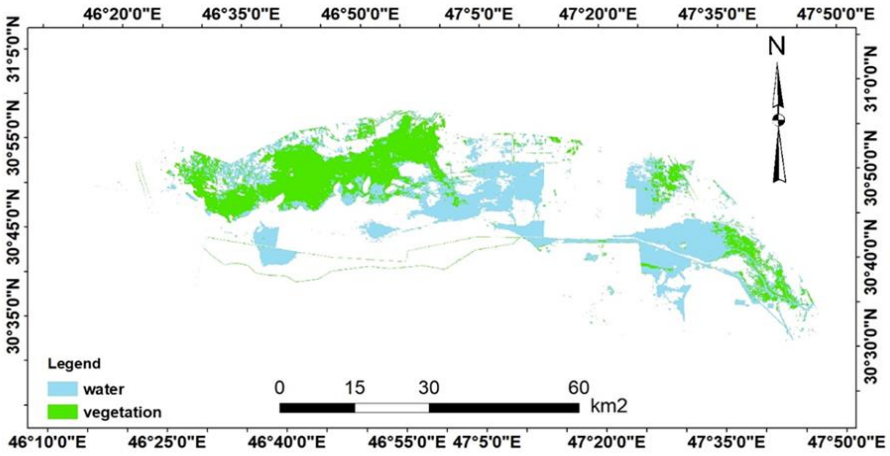

Figure 8. Thematic classification map of the study area for 2015. Water area decreased to 765.98 km^2 while vegetation covered 566.33 km^2, reflecting reduced inflow and drought conditions.

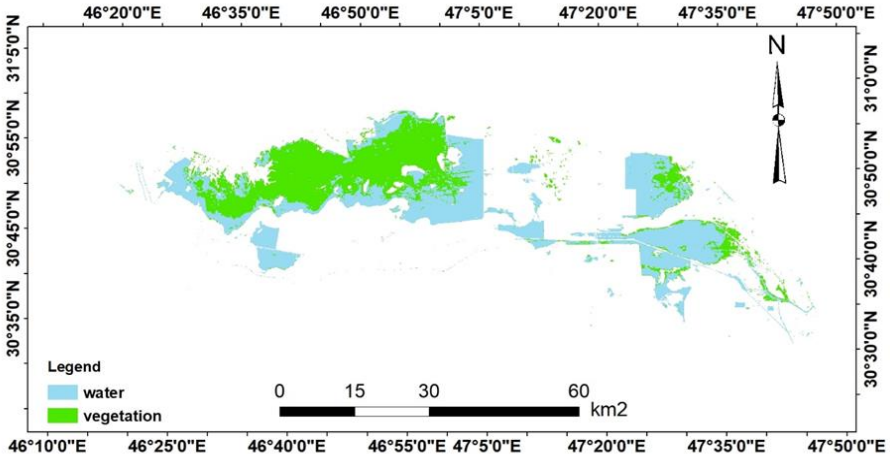

Figure 9. Thematic classification map of Al-Hammar Marsh for 2016. Water (747.73 km^2) and vegetation (572.14 km^2) show a slight decrease in water compared to 2015

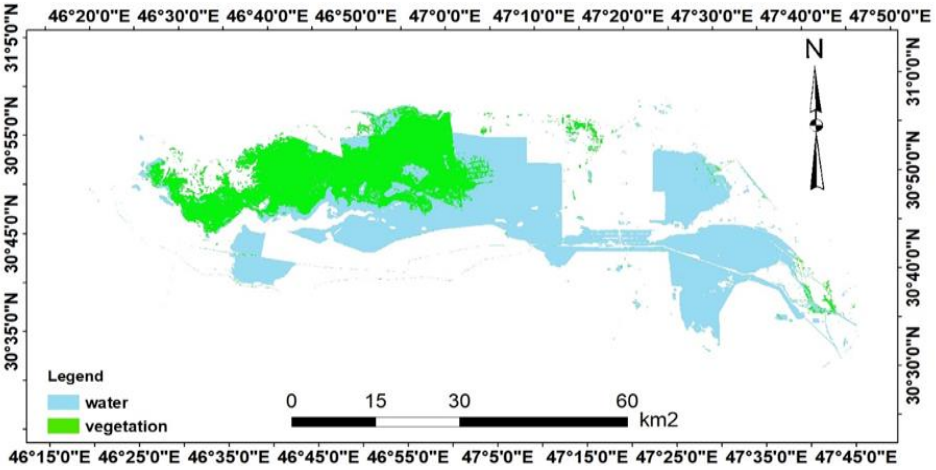

Figure 10. Thematic classification map of Al-Hammar Marsh for 2017. Water (545.10 km^2) and vegetation (624.34 km^2) show continued water reduction and slight vegetation increase.

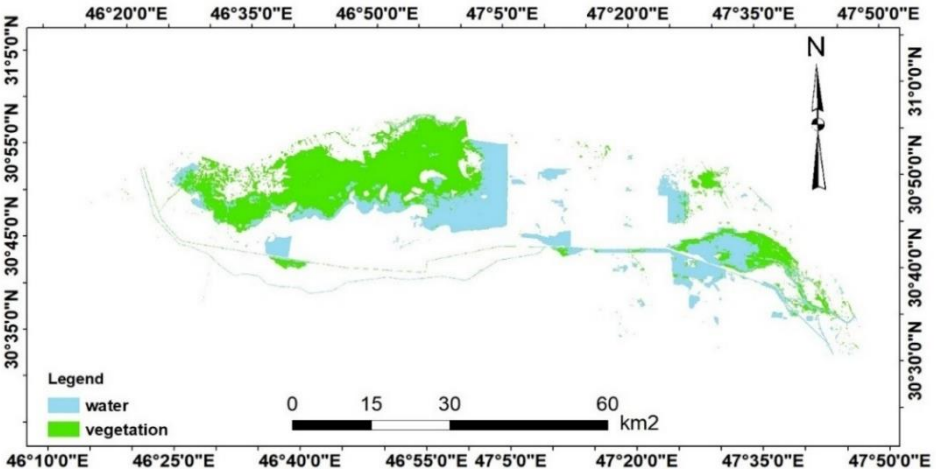

Figure 11. Thematic classification map of Al-Hammar Marsh for 2018. Water area further decreased to 487.61 km^2, and vegetation increased to 652.05 km^2, indicating drying conditions due to water outlet closures.

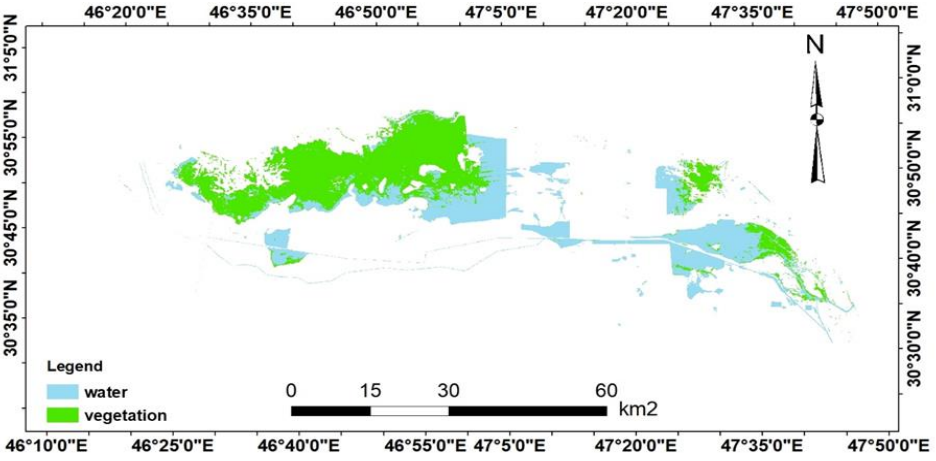

Figure 12. Thematic classification map of Al-Hammar Marsh for 2019. Water area sharply increased to 1144.25 km^2 due to high rainfall, while vegetation remained stable at 642.26 km^2

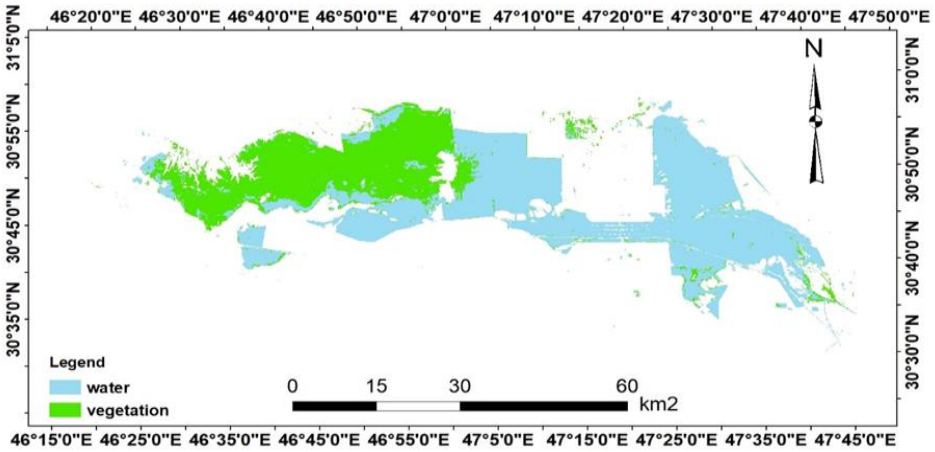

Figure 13. Thematic classification map of the study area for (2020). Water (1128.84 km^2) and vegetation (617.67 km^2) show a minor decrease in vegetation after the 2019 peak.

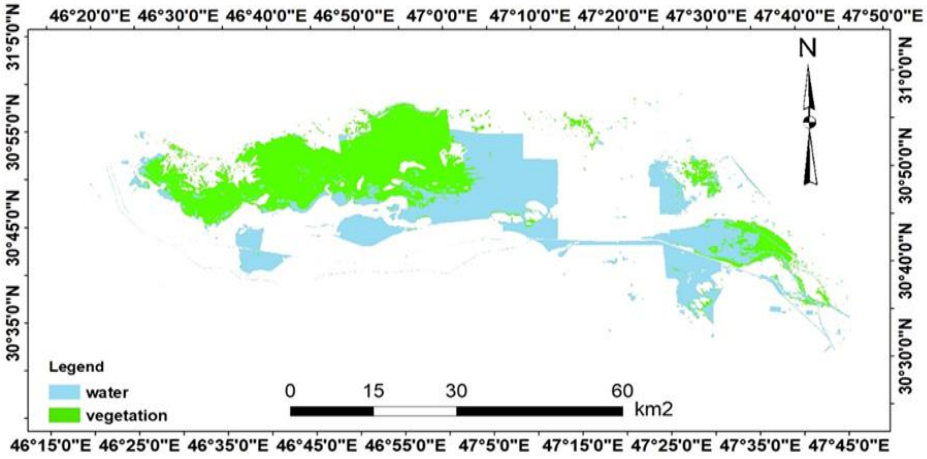

Figure 14. Thematic classification map of Al-Hammar Marsh for 2021. Water (754.25km^2) and vegetation (716.87 km^2) depict significant water reduction with gradual vegetation growth.

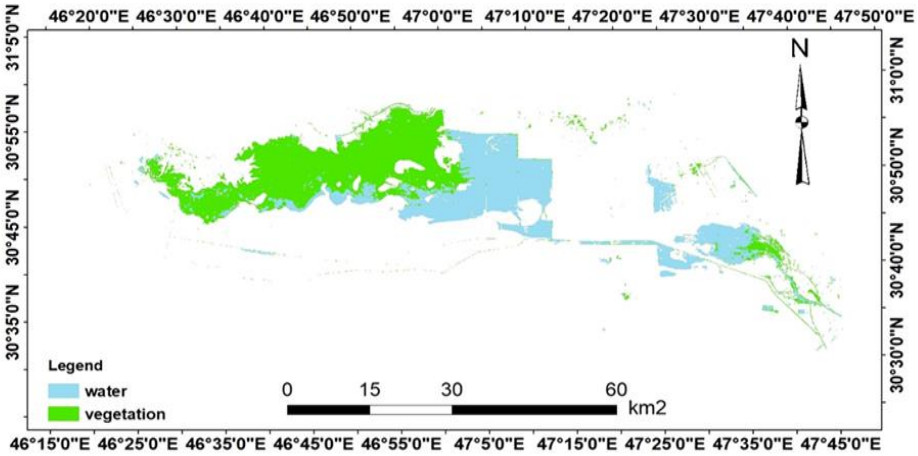

Figure 15. Thematic classification map of Al-Hammar Marsh for 2022. Water reduced to 473.52 km^2, vegetation to 568.92 km^2, reflecting drought conditions.

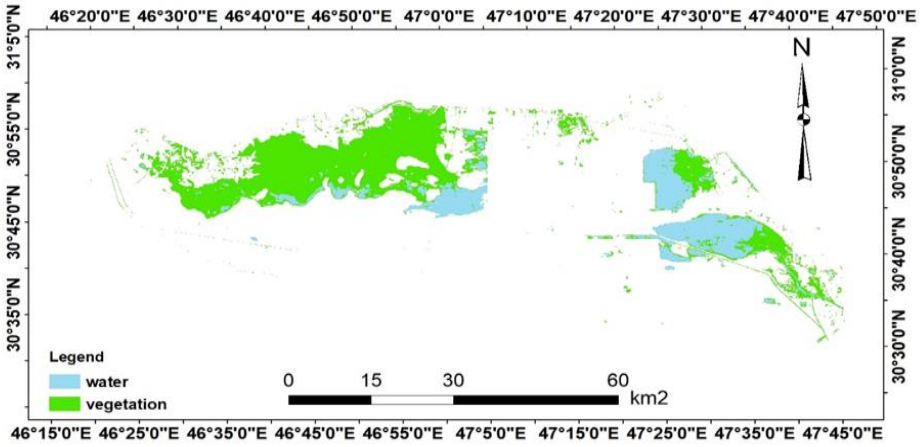

Figure 16. Thematic classification map of Al-Hammar Marsh for 2023. Water area reached the lowest value of 294.33 km^2, while vegetation peaked at 721.43 km^2, indicating extreme drying and concentration of vegetation.

Overall, the maps indicate substantial year-to-year variation in surface-water extent. The increase in water generates positive ecological and socio-economic outcomes, such as supporting biodiversity and sustaining local livelihoods, as observed in 2019 **Fig. 13**, when exceptional rainfall caused a notable expansion of wetland extent. In contrast, reductions in water areas contribute to land degradation and loss of wildlife habitats, as seen in 2018 and 2023 **Figs. 11 and 16**, during which inflow restrictions and limited rainfall resulted in extensive drying.

A simple linear trend analysis **Fig. 17** indicates that while water area experienced high inter-annual variability, vegetation cover shows a moderately increasing trend over the same period. This highlights the dynamic nature of wetland ecosystems, influenced by:

- Hydrological system: Variations in river discharge, rainfall, and inflow from tributaries.
- Climate variability: Droughts and increased rainfall significantly affect water levels, while high temperatures increase evaporation .
- Human activities: Water management, agriculture, drainage projects, and oil extraction impact marsh dynamics.
- Natural vegetation growth: Contributes to changes in land cover independently of water availability.

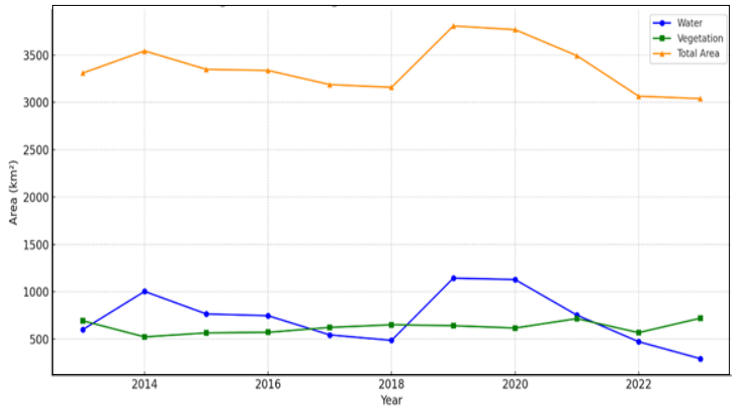

Figure 17. Annual changes in water and vegetation area in Al-Hammar Marsh (2013–2023).

Table 1 demonstrates that the water and vegetation areas in the marshes fluctuate considerably over the years. Overall, increases in water area, such as in 2019, support ecological balance and socioeconomic benefits, whereas decreases, observed in 2015, 2018, and 2023, result in land degradation and loss of wildlife resources, affecting local livelihoods .

Table 1. The areas of Al-Hammar are classified into two classifications in square kilometers

Year	Water in km²	Vegetation in km²	Total area in km²
2013	601.9074	693.9747	3308.882
2014	1004.279	523.9809	3542.26
2015	765.9846	566.3304	3347.315
2016	747.7344	572.1417	3335.876
2017	545.0985	624.3426	3186.441
2018	487.6065	652.0464	3157.653
2019	1144.247	642.258	3805.505
2020	1128.841	617.6727	3766.514
2021	754.2468	716.8725	3492.119
2022	473.5242	568.9233	3064.448
2023	294.3279	721.4256	3038.754

Results of the accuracy assessment in **Table 2** shows high reliability of the classification maps, with kappa coefficients ranging from 0.6854 to 0.9667 and overall accuracy (OA) between 0.87 and 0.98. According to **(Lillesand et al., 2015),** these values indicate a strong agreement between the classified results and reference data, confirming the validity of the analysis.

Table 2. Accuracy index of classification maps.

Images	Accuracy Index	
	Overall Accuracy (OA)	**Kappa Coefficients**
2013	0.95	0.9018
2014	0.94	0.8855
2015	0.87	0.6854
2016	0.93	0.9000
2017	0.94	0.8833
2018	0.94	0.9167
2019	0.98	0.9667
2020	0.97	0.9500
2021	0.98	0.9667
2022	0.96	0.9333
2023	0.97	0.9500

As far as **(Lillesand et al., 2015)**, the value of the kappa coefficient ranges between 0 and 1, while if it is equal to "0", this indicates a large discrepancy between the classification outputs and the reference data. Conversely, there is a strong agreement if the value is equal to (1). However, if the result is between (0.4 and 0.8), the accuracy is average, and a low number is related to random classification.

Comparison with previous studies shows similar patterns of marsh dynamics: **(Al-Maliki et al., 2022)** reported water area fluctuations in southern Iraq marshes due to hydrological changes, while **(Dhaidan et al., 2021)** emphasized the impact of rainfall variability and

human interventions on vegetation cover. The present results align with these findings, demonstrating that the marshes' surface water and vegetation are highly sensitive to environmental and anthropogenic factors.

4. CONCLUSIONS

The marsh's water surface area significantly decreased from 601.9 km^2 in 2013 to 294.3 km^2 in 2023, a decrease of about 51%. In 2019, the water area reached 1144.2 km^2, a 135 % increase over 2018. The year's exceptionally high rainfall was the main cause of this remarkable growth. However, vegetation cover showed a comparatively steady rise during the research period, with a small overall increase of almost 4 %, rising from 693.9 km^2 in 2013 to 721.4 km^2 in 2023. Strong accuracy metrics validated the land cover classification's dependability; the kappa coefficients ranged from 0.68 to 0.96, suggesting a high degree of classification confidence, and the overall accuracy values ranged from 0.87 to 0.98.
These quantitative findings highlight the marsh ecosystem's extreme sensitivity to seasonal hydrological inputs, rainfall variability, and upstream water control. Therefore, it is advised that future research use hydrological and climate modeling techniques to forecast long-term marsh dynamics under various water supply scenarios.

Credit Authorship Contribution Statement

Dina Ali: Writing – original draft, Software. Alaa D. Salman: supervisor, Validation, Methodology.

Declaration of Competing Interests

The authors declare that they have no known competing financial interests or personal relationships that could have appeared to influence the work reported in this paper.

REFERENCES

Abburu, S. and Golla, S.B., 2015. Satellite image classification methods and techniques: A review. *International Journal of Computer Applications*, 119(8), pp. 20–25. https://doi.org/10.5120/21088-3779

Al-Atbee, R.S.K., Al-Hejuje, M.M., and Al-Saad, H.T., 2019. Heavy elements accumulation in dominant aquatic plants at Al-Chibayish Marshes, South of Iraq. *Mesopotamian Journal of Marine Sciences*, 34(2), pp. 154–164. https://doi.org/10.58629/mjms.v34i2.35

Al-Maliki, S., Ibrahim, T., Jakab, G, Masoudi, M., Makki, J., Vekerdy, Z., 2022. An approach for monitoring and classifying marshlands using multispectral remote sensing imagery in arid and semi-arid regions. *Water*, 14(10), P. 1523. https://doi.org/10.3390/w14101523.

Al-Rubaie, A.A.K., 2008. Ecological and morphological study of Iraqi Southern marshes. *Mesopotamian Journal of Marine Science*, 23(2), pp. 437-453.

Aqrawi, A.A.M. and Evans, G.,1994. Sedimentation in the lakes and marshes (Ahwar) of the Tigris-Euphrates Delta, southern Mesopotamia. *Sedimentology*, 41(4), pp. 755–776. https://doi.org/10.1111/j.1365-3091.1994.tb01422.x.

Babu, B.S., 2016. Comparative study on the spatial interpolation techniques in GIS. *International Journal of Scientific & Engineering Research*, 7(2), pp. 550–554. https://doi.org/10.31026/j.eng.2025.08.04.

Campbell, J.B. and Wynne, R.H., 2011. Introduction to remote sensing. *Guilford Press*. https://doi.org/10.3390/rs5010282.

Childs, C., 2004. Interpolating surfaces in ArcGIS Spatial Analyst. *ArcUser, July-September*, 3235(569), pp. 32–35.

Congalton, R.G., 1991. A review of assessing the accuracy of classifications of remotely sensed data. *Remote sensing of environment*, 37(1), pp. 35–46. https://doi.org/10.1016/0034-4257(91)90048-B.

Davidson, N.C., Fluet-Chouinard, E., and Finlayson, C.M., 2020. Global extent and distribution of wetlands: trends and issues. *Marine and Freshwater Research,* 71(6). https://doi.org/10.1071/MF17019.

Dhaidan, B.A., Alwan, I.A., and Al-Khafaji, M.S., 2021. Utilization of satellite image-based indices for assessment of Al-Hammar Marsh restoration plan. *Engineering and Technology Journal*, 39(08), pp. 1328–1337. https://doi.org/10.30684/etj.v39i8.2149.

Dhingra, S. and Kumar, D., 2019. A review of remotely sensed satellite image classification. *International Journal of Electrical and Computer Engineering*, 9(3), P. 1720.

Ghobadi, Y., Pardhan, B.K., Pirasteh, S., Shafri, H.Z.M., Sayyad, G.A., 2012. Use of multi-temporal remote sensing data and GIS for wetland change monitoring and degradation. *IEEE Colloquium on Humanities, Science and Engineering (CHUSER)*, pp. 103–108. https://doi.org/10.1109/CHUSER.2012.6504290.

Hu, T., Sun, L., and Zhang, X., 2021. Mapping surface water dynamics using Landsat time-series data. *Remote Sensing of Environment,* 252, 112–123. https://doi.org/10.3390/rs14102475.

Hussein, Z.E., Hasan, R.H., and Aziz, N.A., 2018. Eh MaDetecting the changes of Al-Hawizrshland and surrounding areas using GIS and remote sensing techniques. *Association of Arab Universities Journal of Engineering Sciences*, 25(1), pp. 53–63.

Irons, J.R., Dwyer, J.L., and Barsi, J.A., 2012. The next Landsat satellite: The Landsat data continuity mission. *Remote Sensing of Environment*, 122, pp. 11–21. https://doi.org/10.1016/j.rse.2011.08.026.

Jenness, J. and Wynne, J.J., 2006. Kappa analysis (kappa_stats. avx) extension for ArcView 3. X. *Jenness Enterprises* http://www.jennessent.com/arcview/kappa_stats.htm.

Jensen, J. R., and Lulla, K., 1987. Introductory digital image processing: A remote sensing perspective. *Geocarto International*, *2*(1), P. 65. https://doi.org/10.1080/10106048709354084.

Jonsson, L., 2015. Evaluation of pixel-based and object-based classification methods for land cover mapping with high spatial resolution satellite imagery, in the Amazonas, Brazil. *Student thesis series INES*.

Lillesand, T., Kiefer, R.W. and Chipman, J., 2015. Remote sensing and image interpretation. *Wiley*.

Liu, J.G. and Mason, P.J., 2016. Image processing and GIS for remote sensing: Techniques and applications. *John Wiley & Sons*. https://doi.org/10.1002/9781118724194.

Malekmohammadi, B. and Blouchi, L.R., 2014. Ecological risk assessment of wetland ecosystems using multi-criteria decision making and geographic information systems. *Ecological Indicators*, 41, pp. 133–144. https://doi.org/10.1016/j.ecolind.2014.01.038.

Meng, H., Zhang, J., and Zheng, Z., 2022. Retrieving inland reservoir water quality parameters using Landsat 8-9 OLI and Sentinel-2 MSI sensors with empirical multivariate regression. *International Journal of Environmental Research and Public Health*, 19(13), P. 7725. https://doi.org/10.3390/ijerph19137725.

Muhsin, I.J., 2017. Monitoring of the South Iraq marshes using classification and change detection techniques. *Iraqi Journal of Physics*, 15(33), pp. 78–86. https://doi.org/10.30723/ijp.v15i33.143.

Nizeyimana, E., 2005. Remote Sensing and GIS Integration. *Encyclopedia of Soil Science, Second Edition*.

Phiri, D., Morgenroth, J., Xu, C. and Hermosilla, T., 2019. Effects of pre-processing methods on Landsat OLI data classification. *Remote Sensing,* 11(3), pp. 1–21. https://doi.org/10.1016/j.jag.2018.06.014.

Richards, J.A. and Jia, X., 2006, Remote sensing digital image analysis: an introduction. *Springer*. https://doi.org/10.1007/3-540-29711-1.

Roy, D.P., Li, J., Zhang, H.K. and Wulder, M.A., 2022. Landsat-9: Continuing the Landsat legacy. *Remote Sensing of Environment*, 269, pp. 112–860. https://doi.org/10.1016/j.rse.2022.113195.

Sabaa, M.R., Salman, A.D., Dakhil, A.J., Jawad, S.I., Karkush, M.O., 2023. Production thematic maps of bearing capacity of shallow foundation for Al-Basrah soil using standard penetration data and GIS. *Journal of Rehabilitation in Civil Engineering*, 11(4), pp. 77–90. https://doi.org/10.22075/JRCE.2023.27587.1668.

Saleh, S.A.H., 2012. Studying of the environmental changes in marsh area using Landsat satellite images. *Journal of Asian Scientific Research*, 2(8), P. 427.

Schowengerdt, R.A., 2006. Remote sensing: models and methods for image processing. *Elsevier*.

Shimal, M.S. and Shaban, A.H., 2019. Estimation of groundwater pollution in Baiji/Salah Al-Deen province, Iraq. AIP Conference Proceedings, 2123(1), P. 020058.

Singh, A., 1989. Review article digital change detection techniques using remotely-sensed data. *International journal of remote sensing*, 10(6), pp. 989–1003. https://doi.org/10.1080/01431168908903939.

Sisodia, P.S., Tiwari, V. and Kumar, A., 2014. A comparative analysis of remote sensing image classification techniques. *International Conference on Advances in Computing, Communications and Informatics (ICACCI)*. IEEE, pp. 1418–1421. https://doi.org/10.1109/ICACCI.2014.6968245.

Soliman, O.S. and Mahmoud, A.S., 2012. A classification system for remote sensing satellite images using support vector machine with non-linear kernel functions. *2012 8th International Conference on Informatics and Systems (INFOS)*. IEEE, P. BIO-181.

Storey, J., Choate, M. and Lee, K., 2014. Landsat 8 Operational Land Imager on-orbit geometric calibration and performance. *Remote sensing*, 6(11), pp. 11127–11152. https://doi.org/10.3390/rs61111127.

Wahaab, H.R., Sultan, M.A., and Aldeen, S.S.S., 2022. Determination of Environmental Factors on some Water and Sediments Quality Parameters of Eastern Al-Hammar Marsh. *IOP Conference Series: Earth and Environmental Science*. IOP Publishing, P. 12034.

Xiao, Y., Lim, S.K., Tan, T.S., 2004. Feature extraction using very high-resolution satellite imagery. *IGARSS 2004. 2004 IEEE International Geoscience and Remote Sensing Symposium*. IEEE. https://doi.org/10.1109/IGARSS.2004.1370741.

Xu, L., He, Z., Zhang, S., and Guo, Y., 2009. The comparative study of three methods of remote sensing image change detection. *The international archives of the photogrammetry, remote sensing and spatial information sciences*, 37(B7). https://doi.org/10.1109/GEOINFORMATICS.2009.5293490

Yacoub, S., Purser, B., Al-Hassani, N., Al-Azzawi, M., Orzag-Sperber, F., Hassan, K., Plaziat, J., Younis, W.,1981. Preliminary study of the Quaternary sediments of SE Iraq. *Joint research project by the Geological Survey of Iraq and University of Paris XI, Orsay, GEOSURV,* int. rep (1981) (1078).

دراسة التغيرات السطحية لهور الحمار من خلال صور الأقمار الصناعية باستخدام تقنيات الاستشعار عن بعد ونظم المعلومات الجغرافية

دينا علي جاسم*، علاء داوود سلمان

قسم هندسة المساحة، كلية الهندسة، جامعة بغداد، بغداد، العراق

الخلاصة

تهدف هذه الدراسة إلى تحليل تقلبات مستويات المياه من خلال حساب مساحة سطح أهوار الحمار في جنوب العراق على مدى 11 عامًا (2013–2023) نظرًا لتوافر بيانات متسقة من القمر الصناعي Landsat–8 وLandsat–9 ولأنها تمثل سنوات ذات تقلبات هيدرولوجية ملحوظة في جنوب العراق، مما يتيح تقييمًا موثوقًا للتغيرات السطحية في أهوار الحمار. باستخدام تقنيات الاستشعار عن بُعد ونظم المعلومات الجغرافية، تم تحديد التغيرات التي طرأت على أهوار الحمار على مدى عقد من الزمن، وذلك بتطبيق أسلوب التصنيف الخاضع للإشراف (الاحتمالية القصوى) لتصنيف المنطقة. وتم تحديد نوعين من الغطاء الأرضي (الماء والنباتات) باستخدام برنامج ArcMap. ثم استُخدمت الخرائط الناتجة لتصنيف الغطاء الأرضي باستخدام البرنامج نفسه. أشارت النتائج إلى تغير كبير في مساحة المستنقع خلال سنوات الدراسة، حيث سُجلت أكبر مساحة مغطاة بالمياه عام 2019 (1144 كم²) وأصغرها عام 2023 (294 كم²). وأظهر تقييم الدقة أن التصنيف الخاضع للإشراف حقق موثوقية عالية، إذ تراوحت قيم الدقة الإجمالية بين 87% و98%، وتراوحت معاملات كابا بين 0.87 و0.98، مما يدل على توافق قوي بين نتائج التصنيف والبيانات المرجعية.

الكلمات المفتاحية: صور الأقمار الصناعية، طريقة التصنيف الخاضعة للإشراف، مساحة السطح.